Commun Nonlinear Sci Numer Simulat 58 (2018) 287–302

Contents lists available at ScienceDirect

Commun Nonlinear Sci Numer Simulat

journal homepage: www.elsevier.com/locate/cnsns

Research paper

Coupled chaotic fluctuations in a model of international trade and innovation: Some preliminary results

Iryna Sushko[a,b,*], Laura Gardini[c], Kiminori Matsuyama[d]

[a] Institute of Mathematics, NASU, Ukraine
[b] Kyiv School of Economics, Ukraine
[c] Dept. of Economics, Society and Politics, University of Urbino, Italy
[d] Dept of Economics, Northwestern University, USA

ARTICLE INFO

Article history:
Available online 23 June 2017

Keywords:
Two-dimensional noninvertible piecewise smooth map
A two-country model of trade and product innovation
Skew tent map
Border collision bifurcation
Bifurcation scenarios

ABSTRACT

We consider a two-dimensional continuous noninvertible piecewise smooth map, which characterizes the dynamics of innovation activities in the two-country model of trade and product innovation proposed in [7]. This two-dimensional map can be viewed as a coupling of two one-dimensional skew tent maps, each of which characterizes the innovation dynamics in each country in the absence of trade, and the coupling parameter depends inversely on the trade cost between the two countries. Hence, this model offers a laboratory for studying how a decline in the trade cost, or globalization, might synchronize endogenous fluctuations of innovation activities in the two countries. In this paper, we focus on the bifurcation scenarios, how the phase portrait of the two-dimensional map changes with a gradual decline of the trade cost, leading to border collision, merging, expansion and final bifurcations of the coexisting chaotic attractors. An example of peculiar border collision bifurcation leading to an increase of dimension of the chaotic attractor is also presented.

1. Introduction

To investigate how globalization might affect the co-movement of innovation activities across countries, Matsuyama et al. [7] developed a two-country model of trade and product innovation, and showed that the innovation dynamics of this two-country model is characterized by a *two-dimensional* (2D for short) *continuous noninvertible piecewise* map: F: $(x, y)\mapsto F(x, y)$, where $x > 0$ and $y > 0$ measure the variety of products that have been innovated in the past and continue to be produced in each country. This map has four parameters, one of which, $\rho \in [0, 1)$, is an inverse measure of the trade cost between the two countries. At a prohibitively high trade cost, the two countries are isolated from each other and $\rho = 0$. In this case, the dynamics of innovation in each country are independent of each other and characterized by a *1D skew tent map* (i.e., a continuous, noninvertible piecewise linear map: see, e.g., [5,6,13]). Furthermore, for the permissible values of the three remaining parameters of this model, each of these two decoupled skew tent maps has a unique attracting fixed point, an attracting period 2 cycle or a 2^i-cyclic chaotic attractor ($i \geq 0$). In this model, a gradual decline in the trade cost causes a gradual market integration of the two countries, or globalization, which is captured by a gradual increase in ρ, leading to a coupling of innovation dynamics in the two countries. Thus, this 2D map offers an ideal laboratory for studying

* Corresponding author at: Institute of Mathematics, NASU, 3 Tereshchenkivska st., 01601 Kyiv, Ukraine.
E-mail addresses: sushko@imath.kiev.ua, ira_sushko@hotmail.com (I. Sushko).

http://dx.doi.org/10.1016/j.cnsns.2017.06.020
1007-5704/

how globalization affects the co-movement of innovation activities across countries. In [7], the analysis of this 2D map was restricted to the case where each of the two decoupled 1D skew tent maps has an attracting cycle of period 2. In this case, the 2D map has at most two coexisting attracting cycles of period 2, "the synchronized 2-cycle" and "the asynchronized 2-cycle". Along the synchronized 2-cycle, product innovation is active and inactive at the same time in the two countries, while it is active only in one country along the asynchronized 2-cycle. It was shown that a gradual increase in ρ causes the basin of attraction of the synchronized 2-cycle to expand and the basin of attraction of the asynchronized 2-cycle to shrink, and that there exists a critical value $\rho_c < 1$, such that the asynchronized 2-cycle is unstable and the synchronized 2-cycle is the only attractor of this 2D system, for $\rho \in (\rho_c, 1)$. Thus, even a partial market integration would cause a full synchronization. Furthermore, it was shown that this critical value ρ_c is lower when the two countries are more unequal in size, which means that a smaller reduction in the trade cost would cause a full synchronization of the innovation activities across the two countries of more unequal size.

In the present paper we continue our investigation of this 2D map by examining the bifurcation scenarios caused by an increase in ρ, including the case where each of the two decoupled 1D skew tent maps has a 2^i-cyclic chaotic attractor ($i \geq 0$). Thus, the decoupled 2D map has 2^i coexisting 2^i-cyclic chaotic attractors, and for increasing ρ some of these attractors disappear and some new attractors appear. In particular, we present examples of so-called *expansion bifurcation* leading to an abrupt increase in the size of a chaotic attractor, *merging bifurcation* associated with direct pairwise merging of the pieces of a chaotic attractor, and *final bifurcation* related to the transformation of a chaotic attractor into a chaotic repellor. As discussed in [1], such bifurcations are caused by a contact of the attractor with its immediate basin boundary which can be regular or fractal. Due to *nonsmoothness* of map F which is defined by four smooth maps in four subregions of the phase plane, so-called *border collision bifurcation* (BCB for short) can also be involved into the bifurcation sequences. Recall that a BCB occurs when the phase portrait of a piecewise smooth map changes qualitatively due to a contact of an invariant set with a border, often called *switching manifold*, along which the system function changes its definition (see [11,13]). The four switching manifolds of the considered map F certainly increase the number of various outcomes of a BCB. In particular, we present an example of a chaotic attractor born due to a BCB, as well as an example of BCB which leads to an increase of dimension of the colliding attractor, namely, cyclic chaotic intervals bifurcate into a cyclic chaotic attractor with Cantor-like structure.

One more important property of the considered map F is its *noninvertibility*. A powerful tool for the investigation of the dynamics of a noninvertible map is the *theory of critical lines* developed in [8] (see also [10]). Recall that a critical line of a 2D continuous noninvertible map is defined as the locus of points having at least two coincident rank-1 preimages. For a 2D *smooth* noninvertible map an image of a set, associated with a vanishing Jacobian determinant, may possess such a property. The considered *piecewise smooth* noninvertible map F has four critical lines each of which is an image of the related switching manifold. We show how these critical lines and their images are used to determine boundaries of chaotic attractors[1] of map F. Critical lines may also be responsible for several interesting transformations of basins of attraction. For example, due to a contact of a basin with a critical line new islands of this basin may appear inside the basin of some other attractor. Similar transformations are described, e.g. in [9]. Recall that in continuous invertible maps the basins of attraction are necessarily simply connected sets, while attractors of noninvertible maps may have connected but not simply connected, or disconnected basins, whose occurrence is related to contact bifurcations with critical lines.

Discussing chaotic attractors of map F we use more general concepts of synchronized and asynchronized fluctuations comparing with those used in [7] for the attracting 2-cycles. Namely, chaotic innovation fluctuations are called synchronized if one observes simultaneous increase or decrease of the values of both variables along the trajectory, and fluctuations are asynchronized if an increase/decrease of the value of one variable is accompanied by a decrease/increase of the value of the other variable.

The paper is organized as follows. In Section 2 we formally introduce map F, briefly explain economics behind it, and discuss its simplest properties. In Section 3 the results related to the dynamics of the skew tent map are applied to the map F for $\rho = 0$. Considering these results as a starting point, in Section 4 we present several bifurcation sequences associated with chaotic attractors, which are observed in the coupled map F when the value of ρ is gradually increased. In case of the countries of equal size discussed in Section 4.1, map F is symmetric with respect to the main diagonal, so that any invariant set S (e.g., an attractor) of F is either symmetric itself, or there exist one more invariant set S' which is symmetric to S. As a results, the bifurcations of coexisting chaotic attractors, which are symmetric to each other with respect to the diagonal, occur simultaneously. In contrast, in the case of the two countries of unequal size, discussed in Section 4.2, map F is asymmetric, and the bifurcations of coexisting chaotic attractors do not occur at the same parameters values, leading to a richer bifurcation scenarios. Section 5 concludes.

[1] Note that chaotic attractors of 2D *invertible* maps, such as, for example, the well known Henon attractor, have a Cantor-like structure, while 2D *noninvertible* maps can have also full measure chaotic attractors.

2. Definition of the map

The family of 2D continuous piecewise smooth maps we study, $F:\mathbb{R}^2_+\to\mathbb{R}^2_+$, is given by the smooth functions F_{HH}, F_{LH}, F_{HL} and F_{LL} defined in the regions D_{HH}, D_{LH}, D_{HL} and D_{LL}, respectively, as follows:

$$F_{LL}:\begin{pmatrix}x\\y\end{pmatrix}\mapsto\begin{pmatrix}f_{LL}(x)=\delta(\theta s_X(\rho)+(1-\theta)x)\\g_{LL}(y)=\delta(\theta s_Y(\rho)+(1-\theta)y)\end{pmatrix}\quad\text{for }(x,y)\in D_{LL},$$

$$F_{HH}:\begin{pmatrix}x\\y\end{pmatrix}\mapsto\begin{pmatrix}f_H(x)=\delta x\\g_H(y)=\delta y\end{pmatrix}\qquad\text{for }(x,y)\in D_{HH},$$

$$F_{HL}:\begin{pmatrix}x\\y\end{pmatrix}\mapsto\begin{pmatrix}f_H(x)=\delta x\\g_{HL}(x,y)=\delta(\theta h_Y(x)+(1-\theta)y)\end{pmatrix}\text{for }(x,y)\in D_{HL},$$

$$F_{LH}:\begin{pmatrix}x\\y\end{pmatrix}\mapsto\begin{pmatrix}f_{LH}(x,y)=\delta(\theta h_X(y)+(1-\theta)x)\\g_H(y)=\delta y\end{pmatrix}\text{for }(x,y)\in D_{LH},$$

where δ, θ and ρ are real parameters satisfying the following conditions:

$$\delta\in(0,1),\quad \theta\in(1,e),\quad \rho\in(0,1);\tag{1}$$

then considering

$$S\in(0,1),\quad s_X=S,\quad s_Y=1-S;$$

for fixed values of ρ and S the values $s_X(\rho)$ and $s_Y(\rho)$ are obtained as follows:

$$s_X(\rho)=\min\left\{\frac{s_X-\rho s_Y}{1-\rho},1\right\},\ s_Y(\rho)=1-s_X(\rho);\tag{2}$$

while the functions $h_X(y)>0$ and $h_Y(x)>0$ are defined from the complementarity slackness conditions

$$\frac{s_X}{h_X(y)+\rho y}+\frac{\rho s_Y}{y+\rho h_X(y)}=1\ \text{ and }\ \frac{s_Y}{h_Y(x)+\rho x}+\frac{\rho s_X}{x+h_Y(x)}=1,$$

respectively, from which we obtain

$$\begin{array}{ll}h_X(y)=\frac{\rho-y(1+\rho^2)+\sqrt{\left(\rho-y(1+\rho^2)\right)^2-4\rho y(\rho y-\rho^2 s_Y-s_X)}}{2\rho} & \text{for }\rho\neq0,\\ h_X(y)=s_X & \text{for }\rho=0,\end{array}\tag{3}$$

and

$$\begin{array}{ll}h_Y(x)=\frac{\rho-x(1+\rho^2)+\sqrt{\left(\rho-x(1+\rho^2)\right)^2-4\rho x(\rho x-\rho^2 s_X-s_Y)}}{2\rho} & \text{for }\rho\neq0,\\ h_Y(x)=s_Y & \text{for }\rho=0.\end{array}\tag{4}$$

The regions D_{LL}, D_{HH}, D_{HL} and D_{LH} are defined as follows:

$$D_{LL}=\{(x,y):x<s_X(\rho),y<s_Y(\rho)\},\ D_{HH}=\{(x,y):x>h_X(y),y>h_Y(x)\},$$

$$D_{HL}=\{(x,y):x>s_X(\rho),y<h_Y(x)\},\ D_{LH}=\{(x,y):x<h_X(y),y>s_Y(\rho)\}.$$

In Fig. 1 the partition of the (x, y)-plane into the regions D_{HH}, D_{LH}, D_{HL} and D_{LL} is illustrated in the symmetric and asymmetric cases, where the blue lines and arrows indicate how the borders of the regions move if the value of ρ increases in the range $0\le\rho\le s_Y/s_X\le1$.

The family of the 2D maps F characterizes the dynamics in the two-country model of trade and product innovation developed by Matsuyama et al. [7], which may be viewed as a hybrid of the closed economy model of product innovation dynamics due to [3] and the two-country model of trade due to [4]. Here, we offer a brief economic interpretation of this map. The reader is referred to [7] for the detailed description of the economic model behind this map as well as for the derivation of this map. There are two countries, X and Y, whose size is given by $s_X=S$ and $s_Y=1-S$, respectively. The states of these economies are summarized by $x>0$ and $y>0$, which measure the variety of products that have been innovated and introduced in the past and are still produced in X and Y, respectively. To this, new products may be added by potential innovators in each country, but they will do so only if they expect to earn enough profit to cover the cost of innovation by selling their new products in both countries. More existing varieties of products in each country, higher x and y, discourage new innovations, but innovators in X are discouraged more by a higher x than a higher y, because new products in X compete directly with the existing products in X but only indirectly with the existing products in Y, due to the trade cost. Likewise, innovators in Y are discouraged more by a higher y than by a higher x. This effect is captured

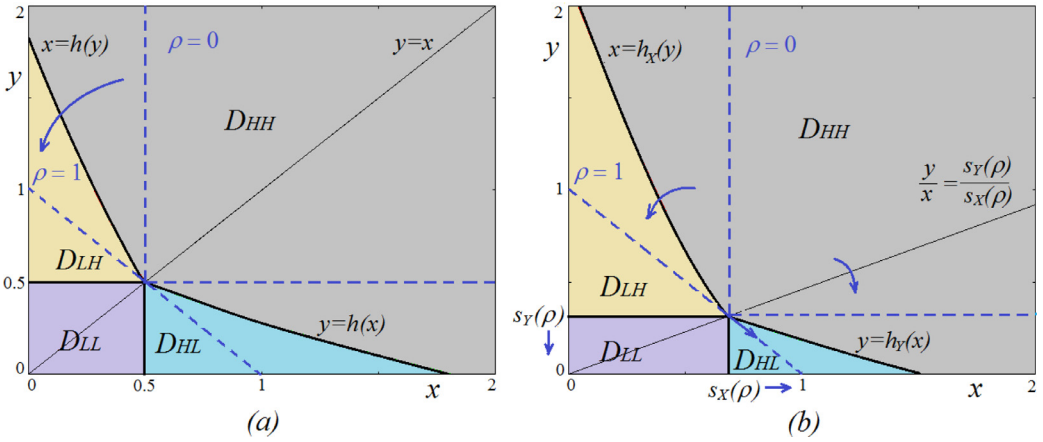

Fig. 1. Partition of the phase plane of map F into the regions D_{HH}, D_{LH}, D_{HL} and D_{LL} in (a) symmetric case ($s_X = s_Y = 0.5$) and (b) asymmetric case ($s_X = 0.6$, $s_Y = 0.4$). The blue arrows indicate how the borders of the regions change if the values of ρ increases in the range $0 \le \rho \le s_Y/s_X \le 1$. (For interpretation of the references to color in this figure legend, the reader is referred to the web version of this article.)

by $\rho \in [0.1)$, a *degree of globalization*, which can be shown to depend inversely on the trade cost.[2] When the trade cost is prohibitively high, $\rho = 0$, and innovation in X is not affected by y, and innovation in Y is not affected by x. When the trade cost approaches to zero, $\rho \to 1$ and innovation in both countries becomes affected by x and y only through its sum, $x + y$. New products also compete with other new products, but the existing products are more discouraging than other new products because the existing products are sold at lower prices. This effect is captured by $\theta \in (1, e)$.[3] Also, any products, both existing and new, become obsolete and stop being produced with probability equal to $0 < 1 - \delta < 1$.[4] The system thus depends on the four parameters S, ρ, θ and δ.

Notice that the state space, $\mathbb{R}^2_+$, is divided into four subregions, within each of which the map is smooth, and some simple observations about the dynamics of map F can be made by analyzing each individual map defined in each of these subregions separately.

For $(x, y) \in D_{HH}$, innovation is inactive in both countries, because too many existing products are currently produced in each country, which makes innovation unprofitable in both countries. With no new products and with the survival rate of the existing products, $0 < \delta < 1$, $F_{HH}(x, y) = (\delta x, \delta y)$, hence the map is contracting towards its fixed point at the origin. Given that this fixed point does not belong to the definition region of F_{HH}, it is not a fixed point of F, and any initial point $(x_0, y_0) \in D_{HH}$ leaves this region in a finite number of iterations.

For $(x, y) \in D_{LL}$, innovation is active in both countries, because there are not too many existing products produced in each country. For the fixed point of map F_{LL} defined as

$$(x^*, y^*) = \left(\frac{\delta\theta s_X(\rho)}{1 + \delta(\theta - 1)}, \frac{\delta\theta s_Y(\rho)}{1 + \delta(\theta - 1)} \right),$$

it holds that $(x^*, y^*) \in D_{LL}$, thus, it is a fixed point of F. At this fixed point, x and y stay constant because a flow of new products introduced by innovation is exactly equal to a flow of the existing products that disappear due to obsolescence in each country. Taking into account the conditions given in (1), one can state that this fixed point is an attracting node for $0 < \delta(\theta - 1) < 1$ and a repelling node for $\delta(\theta - 1) > 1$.

For $(x, y) \in D_{HL}$, innovation is inactive in X and active in Y, because x is high enough, while y is low enough, and for $(x, y) \in D_{LH}$, innovation is active in X and inactive in Y, because y is high, while x is low enough. The related maps, F_{LH} and F_{HL}, are *triangular* given that one of their variables, namely, y for F_{LH} and x for F_{HL}, is independent on the other variable. Fixed points of F_{LH} and F_{HL}, which are defined as $(x, y) = (1, 0)$ and $(x, y) = (0, 1)$, respectively, do not belong to the definition regions of F_{LH} and F_{HL}, thus, they are not fixed points of F. It is easy to see that any initial point $(x_0, y_0) \in D_{LH}$ or $(x_0, y_0) \in D_{HL}$ leaves these regions in a finite number of iterations.

In spite of the trivial dynamics of each map F_{LL}, F_{HH}, F_{LH} and F_{HL} taken separately, the asymptotic behaviors of the trajectories of map F in the generic case are not easy to be investigated. However, there are some specific parameter values for which the dynamics of F can be completely described.

[2] In [7], it was shown that, for innovators, competing against one variety of foreign products is equivalent to competing against ρ variety of domestic products.

[3] In [7], it was shown that, for innovators, competing against one variety of existing products is equivalent to competing against θ variety of new products. It was also shown that θ is bounded from above by e.

[4] Hence, δ may be interpreted as the survival rate of each product.

A first particular case is $\rho = 0$, associated with two countries in autarky, when map F is defined by two *decoupled skew tent maps*. Indeed, from (2) to (4) it follows that the borders between the regions are defined by constants, namely, $s_X(\rho) = h_X(y) = s_X$ and $s_Y(\rho) = h_Y(x) = s_Y$. Moreover, the function $f_{LH}(x, y)$ no longer depends on y and function $g_{HL}(x, y)$ does not depend on x: $f_{LH}(x, y) = f_{LL}(x) =: f_L(x)$ and $g_{HL}(x, y) = g_{LL}(y) =: g_L(y)$. Thus, map F is defined by decoupled 1D maps, denoted f and g:

$$F : \begin{pmatrix} x \\ y \end{pmatrix} \mapsto \begin{pmatrix} f(x) \\ g(y) \end{pmatrix}, \tag{5}$$

where f and g are the skew tent maps given by

$$f : x \mapsto \begin{cases} f_L(x) = \delta(\theta s_X + (1-\theta)x), & x \le s_X, \\ f_H(x) = \delta x, & x > s_X, \end{cases} \tag{6}$$

and

$$g : y \mapsto \begin{cases} g_L(y) = \delta(\theta s_Y + (1-\theta)y), & y \le s_Y, \\ g_H(y) = \delta y, & y > s_Y. \end{cases} \tag{7}$$

We will discuss this case of $\rho = 0$ in greater detail in Section 3.

A second particular case is related to the values of ρ satisfying the condition $s_Y/s_X < \rho < 1$. In fact, in such a case from (2) it follows that $s_X(\rho) = 1$, $s_Y(\rho) = 0$, so that the regions D_{LL} and D_{HL} are empty, and map F is defined by the maps F_{LH} and F_{HH} only. Given that $\delta \in (0, 1)$, it holds that $y \to 0$ under the iterations by F_{LH} and F_{HH}, so that the asymptotic dynamics of F is restricted to the x-axis, where it is governed by the skew tent map

$$f_1 : x \mapsto \begin{cases} \delta(\theta + (1-\theta)x), & x \le 1, \\ \delta x, & x > 1. \end{cases} \tag{8}$$

Analogous conclusions hold for $s_X/s_Y < \rho < 1$ when D_{LL} and D_{LH} are empty. This means that, in a highly globalized world, innovation in the smaller country is never profitable, and hence becomes inactive.

A third particular case is associated with the straight line

$$D = \left\{ (x, y) \in \mathbb{R}^2_+ : \frac{y}{x} = \frac{s_Y(\rho)}{s_X(\rho)} \right\} \tag{9}$$

which is invariant for map F. It is easy to see that for any trajectory with an initial point belonging to D, its x- and y-coordinates are governed by the skew tent maps denoted f_d and g_d, respectively:

$$f_d : x \mapsto \begin{cases} \delta(\theta s_X(\rho) + (1-\theta)x), & x \le s_X(\rho), \\ \delta x, & x > s_X(\rho), \end{cases}$$

and

$$g_d : y \mapsto \begin{cases} \delta(\theta s_Y(\rho) + (1-\theta)y), & y \le s_Y(\rho), \\ \delta y, & y > s_Y(\rho). \end{cases}$$

Finally, there is another particular case when $\rho \to 1$ and the dynamics of $z := x + y$ is governed in the limit by the skew tent map of the form (8). The economic intuition behind this case is quite simple: with no trade cost, the two countries become completely unified and behave as a single country.

All the skew tent maps mentioned above have qualitatively the same dynamics because it is determined only by the slopes of their linear branches which are the same for these maps, namely, $a_L := \delta(1-\theta)$ and $a_R := \delta$. However, the parameters s_X, s_Y and ρ influence the quantitative characteristics of the dynamics (such as, for example, the size of the chaotic attractors) which are also important from an economic point of view. So, as a basic skew tent map it is worth to consider the following one:

$$q : x \mapsto \begin{cases} q_L(x) = \delta(\theta s + (1-\theta)x), & x \le s, \\ q_H(x) = \delta x, & x > s, \end{cases} \tag{10}$$

substituting s by the related parameter and considering the corresponding variable when the specific skew tent map is discussed.

The dynamics of the skew tent map is well studied (see an overview in [13]), and in the following we use the related results as a basis for the description of the dynamics of F in the generic case. In particular, we first give a complete description of the possible attractors and their bifurcations for the decoupled map, i.e., for map F at $\rho = 0$. Then we discuss how the increasing value of ρ influences the dynamics, and compare the symmetric ($s_X = s_Y$) and asymmetric ($s_X \neq s_Y$) cases.

3. Decoupled system ($\rho = 0$)

As mentioned above, for $\rho = 0$ the innovation fluctuations in each country are independent on each other, and map F is determined by the decoupled skew tent maps f and g given in (6) and (7). Below we first describe the possible attractors and their bifurcations observed in the generic skew tent map q given in (10), then apply these results for the description of the phase portrait of the decoupled map F given in (5).

3.1. Skew tent map dynamics

A generic skew tent map can have an attracting fixed point, an attracting cycle of any period $n \geq 1$, or m-cyclic chaotic intervals for any $m \geq 1$.[5] With regards to map q the results are summarized in the following

Proposition 1. *The skew tent map q given in (10) for $\delta \in (0, 1)$, $\theta \in (1, e)$ and any $s > 0$ has the following attractors:*

- *an attracting fixed point*

$$x^* = \frac{\delta\theta s}{1+\delta(\theta-1)} \quad \text{if} \quad 0 < \delta < \delta_{DFB1},$$

where at

$$\delta = \frac{1}{\theta-1} =: \delta_{DFB1} \tag{11}$$

the fixed point x^* undergoes a degenerate flip bifurcation*;*

- *an attracting 2-cycle*

$$\{x_{1,2}, x_{2,2}\} = \left\{ \frac{\delta^2\theta s}{1+\delta^2(\theta-1)}, \frac{\delta\theta s}{1+\delta^2(\theta-1)} \right\} \text{ if } \delta_{DFB1} < \delta < \delta_{DFB2}, \tag{12}$$

where at

$$\delta = \frac{1}{\sqrt{\theta-1}} =: \delta_{DFB2} \tag{13}$$

this 2-cycle undergoes a degenerate flip bifurcation*;*

- *attracting 2^i-cyclic chaotic intervals G_{2^i}, $i \geq 1$, if*

$$\delta > \delta_{DFB2} \quad \text{and} \quad \delta_{H2^i} < \delta < \delta_{H2^{i-1}}, \tag{14}$$

where at

$$\delta = \left(\frac{1-(1-\theta)^{(-1)^i}}{(1-\theta)^{2m_{i+1}}} \right)^{2^{-(i+1)}} =: \delta_{H2^i}, \quad m_i = \frac{2^i-(-1)^i}{3}, \tag{15}$$

the first homoclinic bifurcation *of the harmonic 2^i-cycle occurs, causing the merging bifurcation $G_{2^{i+1}} \Rightarrow G_{2^i}$, and at*

$$\delta = \frac{\sqrt{\theta}}{\theta-1} =: \delta_{H1} \tag{16}$$

the first homoclinic bifurcation of the fixed point x^* occurs leading to the merging bifurcation $G_2 \Rightarrow G_1$;

- *a chaotic interval*

$$G_1 = [\delta s, \delta s(\theta + (1-\theta)\delta)] \quad \text{if} \quad \delta_{H1} < \delta < 1.$$

As discussed in [1], the *merging bifurcation* of a $2m$-cyclic chaotic attractor Q_{2m}, $m \geq 1$, of a continuous map is related to pairwise merging of the pieces of the attractor, $Q_{2m} \Rightarrow Q_m$, occurring due to the first homoclinic bifurcation of a repelling cycle with negative eigenvalue, located at the immediate basin boundary of Q_{2m}. For a more detailed description of *degenerate bifurcations* we refer to [12]. It is worth to note only that for $\delta = \delta_{DFB1}$ any point of the interval $[q_H(s), s] \backslash \{x^*\}$ is 2-periodic, and for $\delta = \delta_{DFB2}$ any point of the intervals $[q_H(s), q_H \circ q_L \circ q_H(s)] \backslash \{x_{1,2}\}$ and $[s, q_L \circ q_H(s)] \backslash \{x_{2,2}\}$ is 4-periodic. As one can see, the boundaries of these intervals are images of the border point $x = s =: c_{-1}$. The point $x = q(s) =: c$ is called *critical point* of q, $c = \delta s$, and $x = q^i(s) =: c_i$, $i \geq 1$, is a critical point of rank i. Critical points of proper ranks define the boundaries of the chaotic intervals, for example, the one-piece chaotic attractor G_1 mentioned in Proposition 1 can be represented as $G_1 = [c, c_1]$.

In Fig. 2a the bifurcation curves $\delta = \delta_{DFB1}$, $\delta = \delta_{DFB2}$, and $\delta = \delta_{H2^i}$, $i \geq 0$, are shown in the (θ, δ)-parameter plane. Note that the curves $\delta = \delta_{H2^i}$ for $i \to \infty$ are accumulating to the point $(\theta, \delta) = (2, 1)$. A 1D bifurcation diagram of x versus δ

[5] For the complete description of the bifurcation structure in the skew tent map we refer to [13] (see also [5,6]).

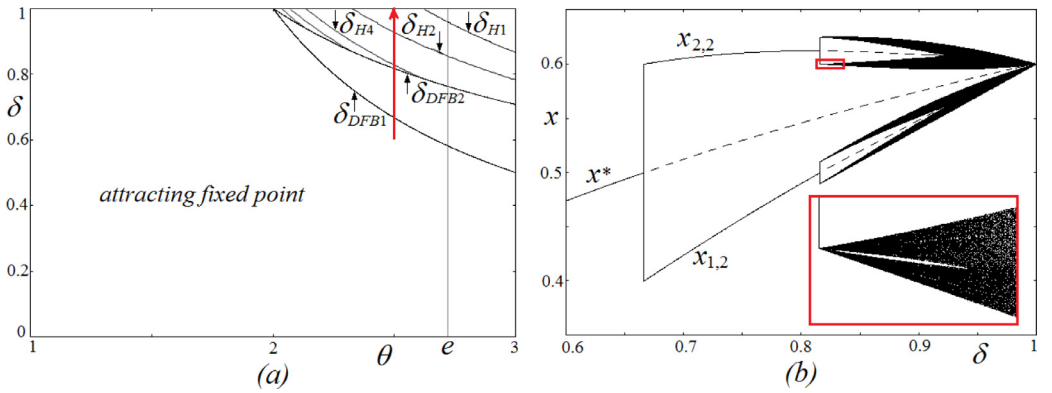

Fig. 2. (a) Bifurcation structure of the (θ, δ)-parameter plane of map q given in (10); recall that the permissible ranges are $0 < \delta < 1$ and $1 < \theta < e$; (b) 1D bifurcation diagram of x versus δ for $0.6 < \delta < 1$ at $\theta = 2.5$ and $s = 0.6$, where the inset shows the indicated rectangle enlarged; dashed lines are related to repelling fixed point and repelling 2-cycle. (For interpretation of the references to color in the text, the reader is referred to the web version of this article.)

obtained for $\theta = 2.5$, $s = 0.6$ is shown in Fig. 2b (the related parameter path is indicated in Fig. 2a by the red arrow). For increasing value of δ such a value of θ is associated with the following cascade of attractors and their bifurcations:

$$x^* \overset{DBF1}{\Rightarrow} \{x_{1,2}, x_{2,2}\} \overset{DBF2}{\Rightarrow} G_8 \overset{H4}{\Rightarrow} G_4 \overset{H2}{\Rightarrow} G_2.$$

Note that the *absorbing interval* $J = [c, c_1] = [\delta s, \delta\theta s + (1-\theta)\delta^2 s]$ of map q shrinks to the point $x = s$ as $\delta \to 1$.

3.2. A 2D view

The phase portrait of the decoupled map F given in (5)–(7) can be seen as a Cartesian product of the phase portraits of maps f and g whose dynamics are qualitatively similar to those described in the previous section. In particular, it is easy to see that if each of the skew tent maps f and g has an n-cyclic attractor (an attracting n-cycle or n-cyclic chaotic intervals) then map F has n coexisting n-cyclic attractors. Based on Proposition 1 we can state that for the related parameter conditions the decoupled map F has either an attracting fixed point, or two coexisting attracting 2-cycles, or 2^i coexisting 2^i-cyclic chaotic attractors (of full measure), $i \geq 0$. Let us present a few examples of such attractors together with their basins.

Consider first the range $\delta_{DFB1} < \delta < \delta_{DFB2}$, where δ_{DFB1} and δ_{DFB2} are given in (11) and (13), respectively, and let the values of the other parameters satisfy the conditions (1). Then the unique fixed point p^* of F defined by

$$(x^*, y^*) = \left(\frac{\delta\theta s_X}{1+\delta(\theta-1)}, \frac{\delta\theta s_Y}{1+\delta(\theta-1)} \right) \tag{17}$$

is repelling, and F has two coexisting attracting 2-cycles, namely, a cycle

$$\{p_{LL}, p_{HH}\} = \{(x_{1,2}, y_{1,2}), (x_{2,2}, y_{2,2})\} \in D,$$

which we call *synchronized* (innovation in the two countries are active and inactive at the same time), and a cycle

$$\{p_{LH}, p_{HL}\} = \{(x_{1,2}, y_{2,2}), (x_{2,2}, y_{1,2})\},$$

called *asynchronized* (innovation is active only in one country). Here the coordinates of the points of the cycles are obtained from (12) substituting $s = s_X$ for the x-coordinates and $s = s_Y$ for the y-coordinates. Besides the repelling fixed point and attracting 2-cycles mentioned above, map F has also two saddle cycles:

$$\begin{aligned} \{p'_{LL}, p'_{LH}\} &= \{(x^*, y_{1,2}), (x^*, y_{2,2})\}, \\ \{p''_{LL}, p''_{HL}\} &= \{(x_{1,2}, y^*), (x_{2,2}, y^*)\}. \end{aligned} \tag{18}$$

The closure of the stable invariant sets of these saddle cycles constitutes the boundary of the basins of attraction of the attracting 2-cycles. In Fig. 3 we present an example of such basins where the branches of the local stable invariant sets of the saddle 2-cycles are also shown.

Suppose now that $\delta > \delta_{DFB2}$ and $\delta_{H2^i} < \delta < \delta_{H2^{i-1}}$, where δ_{H2^i} for $i \geq 1$ is defined in (15) and δ_{H1} in (16). Each of the skew tent maps f and g has 2^i-cyclic chaotic intervals and, thus, the decoupled map F has 2^i coexisting 2^i-cyclic chaotic attractors. Fig. 4a presents four coexisting 4-cyclic chaotic attractors and their basins whose boundaries are formed by the closure of the stable invariant sets of the four saddle 4-cycles (their points are indicated by yellow, orange, black and dark brown circles), and in Fig. 4b two coexisting 2-cyclic chaotic attractors with their basins are shown, which we consider below in more details.

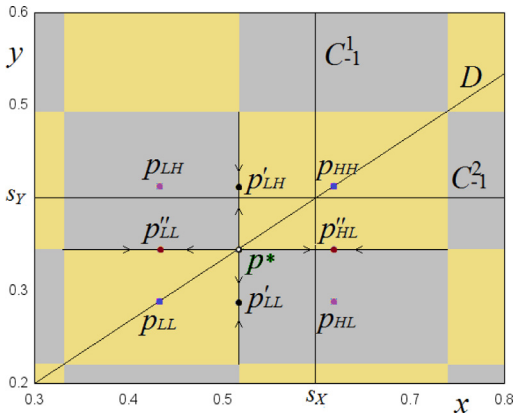

Fig. 3. Attracting 2-cycles $\{p_{LL}, p_{HH}\}$ and $\{p_{LH}, p_{HL}\}$ and their basins separated by the closure of the stable invariant sets of the saddle 2-cycles $\{p'_{LL}, p'_{LH}\}$ and $\{p''_{LL}, p''_{HL}\}$. Here $\theta = 2.7$, $\delta = 0.7$, $s_X = 0.6$, $s_Y = 0.4$.

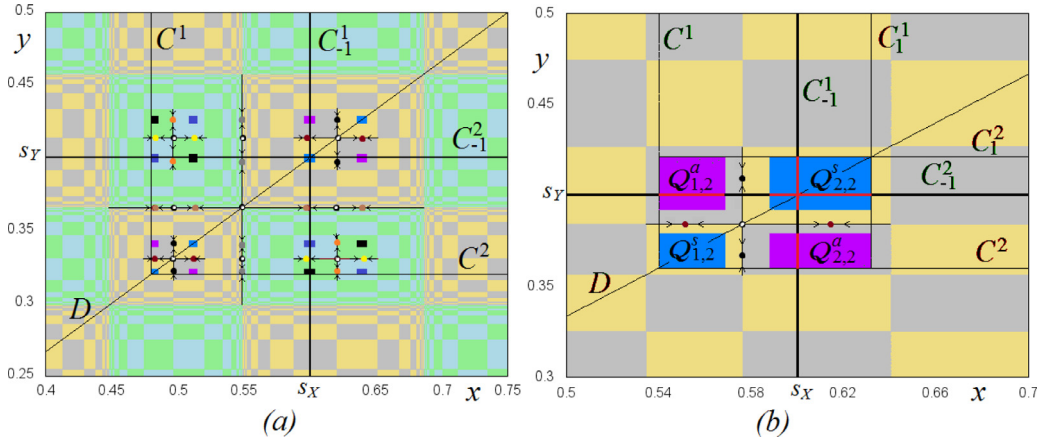

Fig. 4. 2^i coexisting 2^i-cyclic chaotic attractors of the decoupled map F and their basins for $\theta = 2.7$, $s_X = 0.6$, $s_Y = 0.4$ and (a) $\delta = 0.8$, $i = 2$, (b) $\delta = 0.9$, $i = 1$. (For interpretation of the references to color in the text, the reader is referred to the web version of this article.)

The 2-cyclic chaotic attractors shown in Fig. 4b are denoted $Q_2^s = \{Q_{1,2}^s, Q_{2,2}^s\}$ and $Q_2^a = \{Q_{1,2}^a, Q_{2,2}^a\}$. The upper index s in Q_2^s refers to 'synchronized' increase or decrease of the x- and y-coordinates along a trajectory belonging to Q_2^s (i.e. for an initial point (x_0, y_0) belonging to Q_2^s, for the point $(x_1, y_1) = F(x_0, y_0)$ it holds that either $x_1 > x_0$, $y_1 > y_0$ or $x_1 < x_0$, $y_1 < y_0$), while the index a in Q_2^a indicates that these values are 'asynchronized', that is, an increase of the x-coordinate corresponds to a decrease of the y-coordinate, and *vice versa* (i.e., either $x_1 > x_0$, $y_1 < y_0$ or $x_1 < x_0$, $y_1 > y_0$). Similar to the basin boundary of the coexisting 2-cycles shown in Fig. 3, the basin boundary of the 2-cyclic chaotic attractors Q_2^s and Q_2^a is the closure of the stable invariant sets of the saddle 2-cycles $\{p'_{LL}, p'_{LH}\}$ and $\{p''_{LL}, p''_{LH}\}$ defined in (18) and indicated by black and brown circles in Fig. 4b.

The boundaries of the chaotic attractors Q_2^s and Q_2^a can be determined using critical lines of map F. As we already mentioned in the Introduction, the theory of critical lines is quite a powerful tool to describe the dynamics of noninvertible maps (see [8–10]). With some similarity to a critical point (an extremum) of a 1D continuous noninvertible map, a *critical line* C of a 2D continuous noninvertible map G is defined as the locus of points having at least two coincident rank-1 preimages. For a 2D smooth noninvertible map the set $C = G(C_{-1})$, where C_{-1} is a set associated with a vanishing Jacobian determinant, may possess such a property. For a 2D piecewise smooth map the set $C = G(C_{-1})$, where C_{-1} (often called *switching manifold*) is related to a change of the definition of the system function and, thus, to a discontinuity of the Jacobian determinant, is also called critical line. For the considered decoupled map F there are two switching manifolds:

$$C^1_{-1} = \{(x, y) : x = s_X, y > 0\}, \quad C^2_{-1} = \{(x, y) : x > 0, y = s_Y\}.$$

So, the critical lines of F are defined as $C^1 = F(C^1_{-1})$ and $C^2 = F(C^2_{-1})$:

$$C^1 = \{(x, y) : x = \delta s_X, y > \delta s_Y\}, \quad C^2 = \{(x, y) : x > \delta s_X, y = \delta s_Y\},$$

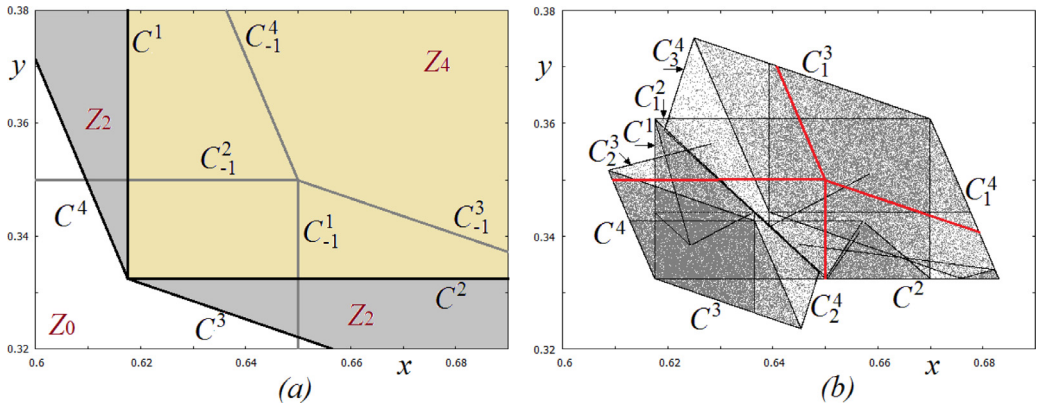

Fig. 5. (a) Critical lines C^i, $i=\overline{1,4}$, of map F, and their preimages C^i_{-1} (critical lines of rank −1). The critical lines C^i separate regions Z_0, Z_2 and Z_4, whose points have 0, 2 and 4 distinct preimages; (b) chaotic attractor of map F and its boundary formed by segments of critical lines of indicated ranks. (For interpretation of the references to color in the text, the reader is referred to the web version of this article.)

and the critical lines of rank i are ith images of C^1 and C^2: $C^1_i = F^i(C^1)$ and $C^2_i = F^i(C^2)$. Indeed, the critical lines of the decoupled map F are determined by the critical points $c^1 = \delta s_X$ and $c^2 = \delta s_Y$ of the skew tent maps f and g, respectively, defined in (6) and (7).

To obtain the boundaries of the chaotic attractors of map F one has to determine the so-called *generating segment(s)* (see [8]) which are the segments of C^1_{-1} and C^2_{-1} belonging to the attractors. A suitable number of images of these generating segments give the boundaries of the chaotic attractors. For example, for the chaotic attractors shown in Fig. 4b there are two couples of generating segments (highlighted in red), $\{J^{1,1}_{-1}, J^{1,2}_{-1}\} \in C^1_{-1}$, and $\{J^{2,1}_{-1}, J^{2,2}_{-1}\} \in C^2_{-1}$:

$$J^{1,1}_{-1} = \{(x,y) : x = s_X, c^2 < y < c^2_2\},\ J^{1,2}_{-1} = \{(x,y) : x = s_X, c^2_3 < y < c^2_1\},$$

$$J^{2,1}_{-1} = \{(x,y) : y = s_Y, c^1 < x < c^1_2\},\ J^{2,2}_{-1} = \{(x,y) : y = s_Y, c^1_3 < x < c^1_1\},$$

where $c^1_i = f^i(c^1)$, $c^2_i = g^i(c^2)$, $i=\overline{1,3}$. Using these critical points all the boundaries of the chaotic attractors are easily determined.

4. Dynamics of the coupled system ($\rho > 0$)

Let us turn to consider map F for $\rho > 0$. The variables are now coupled through the maps F_{LH} and F_{HL}, for which in contrast to the decoupled case, $h_X(y) \neq s_X$ and $h_Y(x) \neq s_Y$. Obviously, due to a smooth dependence of map F on ρ, for values of ρ close to 0 the dynamics of F remains qualitatively similar to the one described in the previous section. In the present one we investigate how the phase portrait of F changes if the value of ρ is gradually increasing.

First, let us determine the critical lines of map F for $\rho > 0$. There are four switching manifolds:

$$C^1_{-1} = \{(x,y) : x = s_X(\rho), 0 < y < s_Y(\rho)\},$$
$$C^2_{-1} = \{(x,y) : y = s_Y(\rho), 0 < x < s_X(\rho)\},$$
$$C^3_{-1} = \{(x,y) : y = h_Y(x), x > s_X(\rho)\},$$
$$C^4_{-1} = \{(x,y) : x = h_X(y), y > s_Y(\rho)\},$$

(see Fig. 1b where the sets C^i_{-1}, $i=\overline{1,4}$, are the boundaries of the regions D_{LL}, D_{LH}, D_{HL} and D_{HH}). Correspondingly, map F has four critical lines:

$$C^1 = \{(x,y) : x = \delta s_X(\rho), y > \delta s_Y(\rho)\},$$
$$C^2 = \{(x,y) : y = \delta s_Y(\rho), x > \delta s_X(\rho)\},$$
$$C^3 = \{(x,y) : y = \delta h_Y(x/\delta), x > \delta s_X(\rho)\},$$
$$C^4 = \{(x,y) : x = \delta h_X(y/\delta), y > \delta s_Y(\rho)\}.$$

These critical lines separate regions whose points have a different number of rank-one preimages (see Fig. 5a): each point of the regions

$$Z_4 = \{(x,y) : x > \delta s_X(\rho), y > \delta s_Y(\rho)\}$$

and

$$Z_2 = \{(x,y) : \delta h_X(y/\delta) < x < \delta s_X(\rho)\} \cup \{(x,y) : \delta h_Y(x/\delta) < y < \delta s_Y(\rho)\}$$

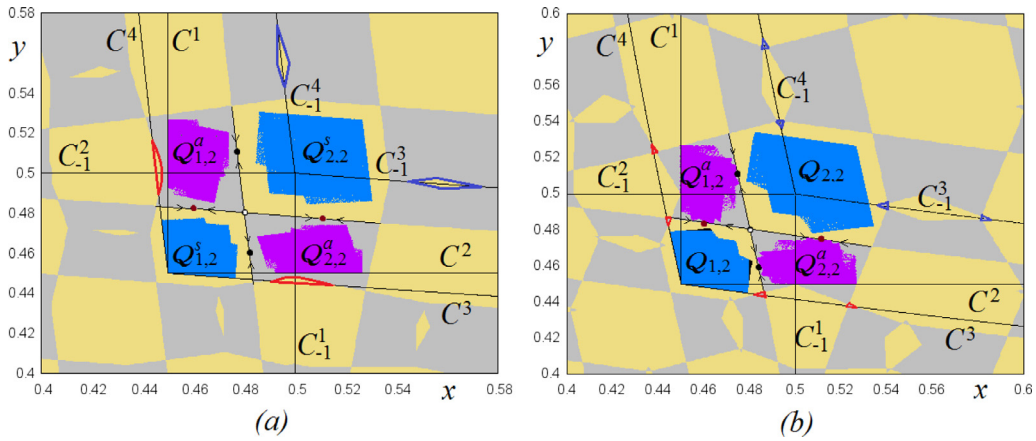

Fig. 6. Coexisting 2-cyclic chaotic attractors and their basins for $s_X = s_Y = 0.5$, $\theta = 2.7, \delta = 0.9$ and (a) $\rho = 0.05$, (b) $\rho = 0.09$. (For interpretation of the references to color in the text, the reader is referred to the web version of this article.)

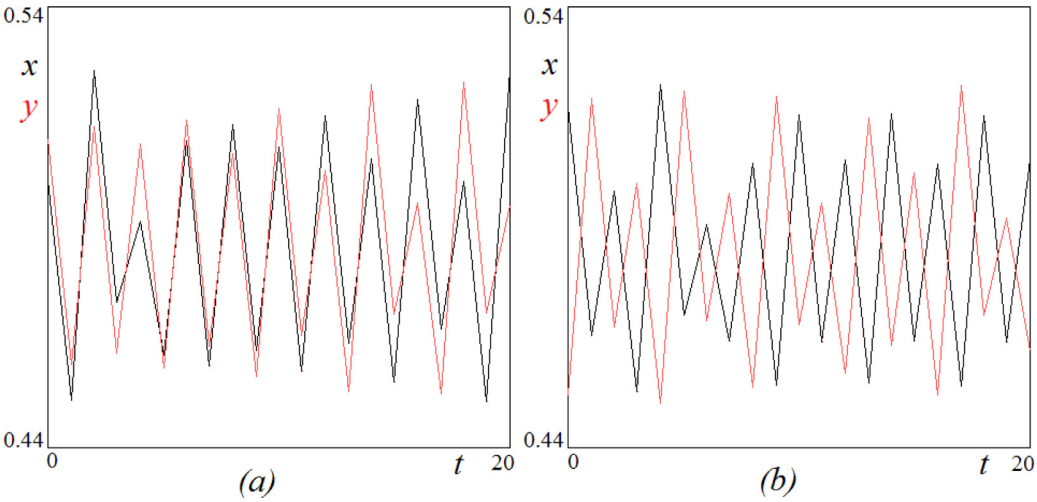

Fig. 7. Time series associated with synchronised attractor Q_2^s (a) and asynchronized attractor Q_2^a (b), where fluctuations of the values of x and y are shown in black and red, respectively. Here parameter values are fixed as in Fig. 6a. (For interpretation of the references to color in this figure legend, the reader is referred to the web version of this article.)

has four and two distinct preimages, respectively, and each point of the region

$$Z_0 = \{(x, y) : x < \delta h_X(y/\delta), y < \delta h_Y(x/\delta)\}$$

has no preimages. Thus, map F has a so-called $Z_0 - Z_2 - Z_4$ type of noninvertibility. As one can see, applying F the phase plane becomes folded along the critical lines, which is a characteristic property of noninvertible maps.

In Fig. 5b we present an example of a chaotic attractor of map F whose boundary is formed by segments of the following critical lines: C^i for $i = \overline{1,4}$, C_1^i for $i = \overline{2,4}$, C_2^i for $i = 3, 4$ and C_3^4, which are images of the generating segments highlighted in red.

4.1. Increasing ρ in the symmetric case ($s_X = s_Y$)

Consider $s_X = s_Y = 0.5$, so that map F is symmetric with respect to the main diagonal, and $\theta = 2.7$, $\delta = 0.9$. It is easy to check that for such values it holds $\delta > \delta_{DFB2}$ and $\delta_{H2} < \delta < \delta_{H1}$ (see (14)), so, according to Proposition 1, map F for $\rho = 0$ has two coexisting 2-cyclic chaotic attractors, a synchronized attractor $Q_2^s = \left\{Q_{1,2}^s, Q_{2,2}^s\right\}$ and an asynchronized attractor $Q_2^a = \left\{Q_{1,2}^a, Q_{2,2}^a\right\}$. Map F has also a repelling fixed point p^* and a pair of saddle 2-cycles defined in (17) and (18), respectively.

For $\rho = 0.05$ map F still has two coexisting 2-cyclic chaotic attractors, a synchronized attractor Q_2^s and an asynchronized attractor Q_2^a (see Fig. 6a). Recall that in case of synchronized chaotic fluctuations the values of both variables along the trajectory increase or decrease simultaneously, and in case of asynchronized fluctuations an increase/decrease of the value of one variable is accompanied by a decrease/increase of the value of the other variable. In Fig. 7a we show a time series

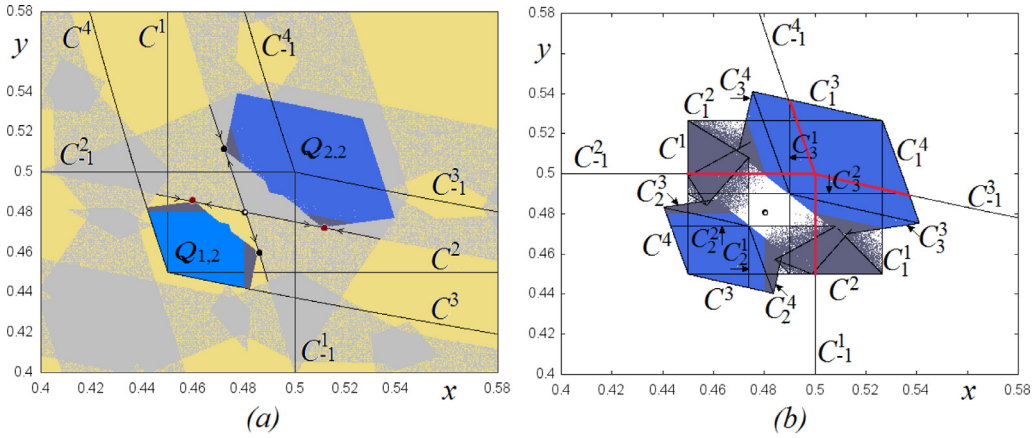

Fig. 8. (a) Two coexisting chaotic attractors of F^2 (corresponding to the 2-cyclic chaotic attractor Q_2 of F) and their basins before, and close to, an expansion bifurcation; (b) an annular chaotic attractor of F after the expansion bifurcation of Q_2. Blue and dark gray parts of the attractors are associated with synchronized and asynchronized dynamics, respectively. Here $s_X = s_Y = 0.5, \theta = 2.7$, $\delta = 0.9$ and (a) $\rho = 0.135$, (b) $\rho = 0.15$. (For interpretation of the references to color in this figure legend, the reader is referred to the web version of this article.)

associated with Q_2^s where one can see simultaneous increase and decrease of x and y shown in black and red, respectively. Fig. 7b presents a time series related to Q_2^a, where an anti-phase movement of the variables is clearly visible.

Basin boundaries of Q_2^s and Q_2^a are formed by the closure of the stable invariant sets of two saddle 2-cycles marked by black and brown circles. However, note that islands of the basin of Q_2^s have appeared inside the basin of Q_2^a. Such a transformation is caused by two symmetric parts of the basin of Q_2^s (their boundaries are highlighted in red in Fig. 6a), which 'entered' the region Z_2 after crossing the critical lines C^3 and C^4, so that new preimages of these parts have appeared. In particular, their first preimages (highlighted in blue) are intersected by the critical lines C^3_{-1} and C^4_{-1}, and belong to the region Z_4, thus, each of these islands has four preimages.

For $\rho = 0.09$ (see Fig. 6b) the attractor Q_2^s is no longer completely synchronized: relatively small parts of this attractor, shown in black, have appeared, associated with asynchronized behavior of the trajectory, so now we denote this attractor as $Q_2 = \{Q_{1,2}, Q_{2,2}\}$ eliminating the index 's'. Note also that there are new islands of the basin of the chaotic attractor Q_2^a inside the basin of the chaotic attractor Q_2, which have appeared following the same mechanism as described above: there are parts of the basin of Q_2^a (highlighted in red) which 'entered' the region Z_2 after crossing the critical lines C^3 and C^4, leading to new preimages, in particular, those intersected by C^3_{-1} and C^4_{-1} (they are highlighted in blue). Note also that the attractor Q_2^a is close to a contact with its immediate basin boundary. After this contact called a *final bifurcation* (see [1,8]), caused by the first (one-side) homoclinic bifurcation of the saddle 2-cycles, the former chaotic attractor Q_2^a is transformed into a chaotic repellor, and the only attractor of F is the chaotic attractor Q_2.

If ρ is further increased, a contact occurs of Q_2 with its immediate basin boundary caused by the (other-side) homoclinic bifurcation of the saddle 2-cycles: at $\rho = 0.135$ the attractor Q_2 is near to such a contact that can be visualized considering the second iterate of F, that is, map F^2, and the basins of its coexisting chaotic attractors $Q_{1,2}$ and $Q_{2,2}$ (see Fig. 8a). Note that for increasing ρ the asynchronized parts of Q_2 marked by dark gray become larger, however, the synchronized behavior still dominates. After the contact of Q_2 with its immediate basin boundary the former chaotic repellor, appeared after the final bifurcation of Q_2^a, reveals itself becoming a part of the new one-piece chaotic attractor Q, so that we observe a sudden increase in size of the attractor called an *expansion bifurcation* (see [1]). In Fig. 8b we present the attractor Q for $\rho = 0.15$, after the expansion bifurcation of Q_2. Note that it has an annular shape that can be verified considering the proper number of images of the generating segments (the boundaries of the attractor shown in Fig. 8b are formed by four images of the generating segments highlighted in red). The synchronized and asynchronized behavior of the trajectory belonging to Q is indicated by blue and dark gray, respectively.

In order to describe further transformations of the attractors and their basins it is more convenient first to consider $\rho = 0.35$, and then we decrease ρ gradually back to $\rho = 0.15$. Map F at $\rho = 0.35$ again has two coexisting attractors, Q_2 and Q_2^a, shown in Fig. 9a together with their basins. In this case the basin boundary is formed by the closure of the stable invariant sets of two saddle 4-cycles (shown by black and brown circles) located on the immediate basin boundary. These cycles are born due to a flip bifurcation of the former saddle 2 -cycles, which are now repelling nodes. Decreasing the value of ρ at first the attractor Q_2 has a contact with its immediate basin boundary (at $\rho \approx 0.338$) and is transformed into a chaotic repellor, then the attractor Q_2^a has a contact with its immediate basin boundary (at $\rho \approx 0.295$) causing an expansion bifurcation and leading to a one-piece simply-connected chaotic attractor Q. If we continue to decrease ρ then the attractor Q is transformed into the annular attractor[6] shown in Fig. 8b for $\rho = 0.15$.

[6] Recall that a transition from a one-piece annular chaotic attractor to a one-piece simply-connected attractor is associated with a *snap-back repellor bifurcation* of the unstable fixed point located in the center of the annular attractor (see, e.g., [2]).

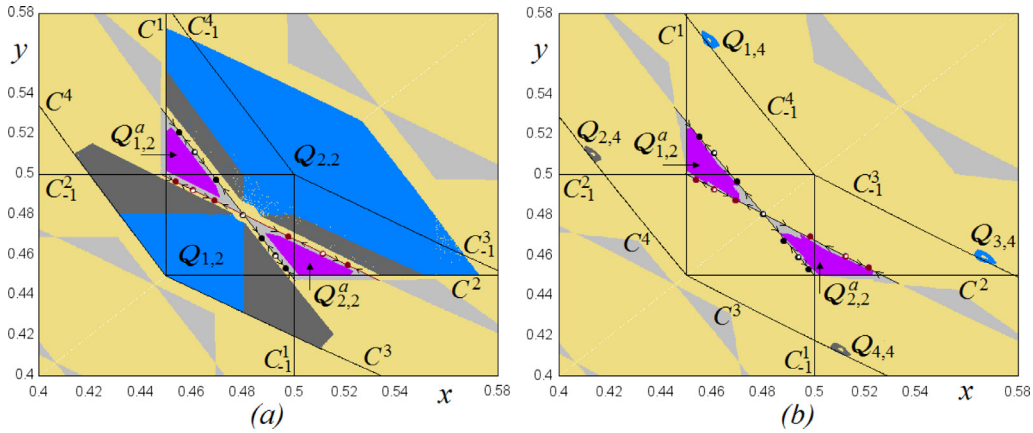

Fig. 9. (a) 2-cyclic chaotic attractors Q_2 and Q_2^a and their basins; (b) 4-cyclic chaotic attractor Q_4 and 2-cyclic chaotic attractor Q_2^a and their basins. The synchronized and asynchronized parts of the attractors Q_2 and Q_4 are shown in blue and dark gray, respectively. Here $s_X = s_Y = 0.5$, $\theta = 2.7$, $\delta = 0.9$ and (a) $\rho = 0.35$, (b) $\rho = 0.38$. (For interpretation of the references to color in this figure legend, the reader is referred to the web version of this article.)

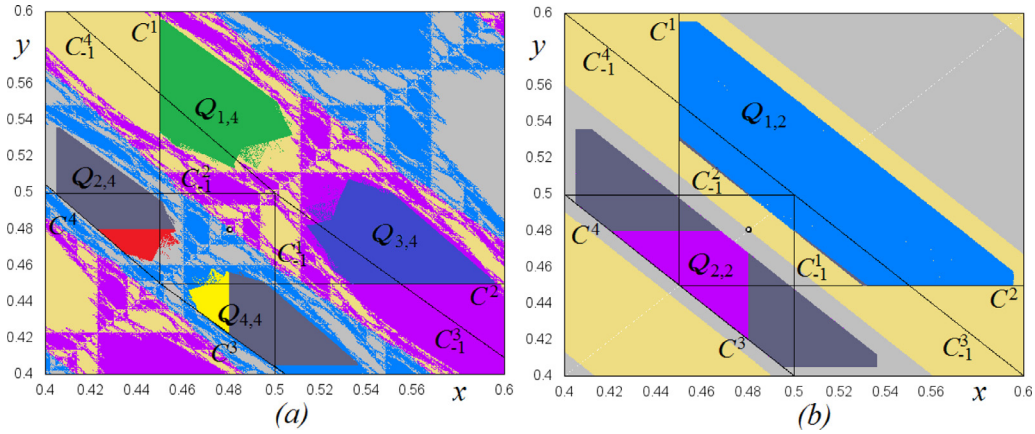

Fig. 10. (a) Four coexisting chaotic attractors $Q_{i,4}$, $i = \overline{1,4}$, of map F^4 (related to the 4-cyclic chaotic attractor Q_4 of F), and their basins; (b) two coexisting chaotic attractors $Q_{1,2}$ and $Q_{2,2}$ of map F^2 (related to the 2-cyclic chaotic attractor Q_2 of F), and their basins. The parts of the attractors of F related to the asynchronized behavior are shown in dark gray. Here $s_X = s_Y = 0.5$, $\theta = 2.7$, $\delta = 0.9$ and (a) $\rho = 0.665$, (b) $\rho = 0.95$.

Now let us continue to increase ρ from $\rho = 0.35$ (see Fig. 9a). At $\rho \approx 0.3563$ a *fold border collision bifurcation*[7] occurs leading to a 4-cyclic annular chaotic attractor $Q_4 = \{Q_{i,4}\}_{i=1}^4$. In Fig. 9b, where $\rho = 0.38$, the attractor Q_4 coexists with the 2-cyclic chaotic attractor Q_2^a, which is close to a contact with its immediate basin boundary. Two parts of Q_4 shown in blue and two parts of Q_4 shown in dark gray are related to the synchronized and asynchronized behavior of the trajectory, respectively. Note that at the BCB mentioned above a pair of 4-cycles is also born, and the points of one 4-cycle are located in the centers of the annular pieces of Q_4, while the points of the other 4-cycle are located at the immediate basin boundary of Q_4.

Increasing ρ further, the attractor Q_2^a undergoes its final bifurcation, while the attractor Q_4 increases in size. In Fig. 10a, where $\rho = 0.665$, the coexisting attractors $Q_{i,4}$, $i = \overline{1,4}$, of F^4 are shown, associated with the 4-cyclic attractor Q_4 of F. It can be seen that the attractor Q_4 is close to a contact with the immediate basin boundary, and the whole boundary has a *fractal structure*. After the contact (causing an expansion bifurcation) map F has a 2-cyclic chaotic attractor $Q_2 = \{Q_{1,2}, Q_{2,2}\}$: in Fig. 10b where $\rho = 0.95$, two coexisting attractors, $Q_{1,2}$ and $Q_{2,2}$, of F^2 (related to the 2-cyclic attractor Q_2 of F) are shown together with their basins. Further increase of ρ up to the limit value $\rho = 1$, does not lead to qualitative changes of the phase portrait of F.

[7] Recall that a*fold BCB*, similar to a 'smooth' fold bifurcation, is associated with a couple of cycles, however, it is related not to an eigenvalue equal to 1, but to a collision of two cycles with a switching manifold. These cycles merge at the moment of collision and disappear (or appear) after. Differently from the smooth fold bifurcation, leading to node and saddle cycles, a fold BCB may lead to two repelling cycles.

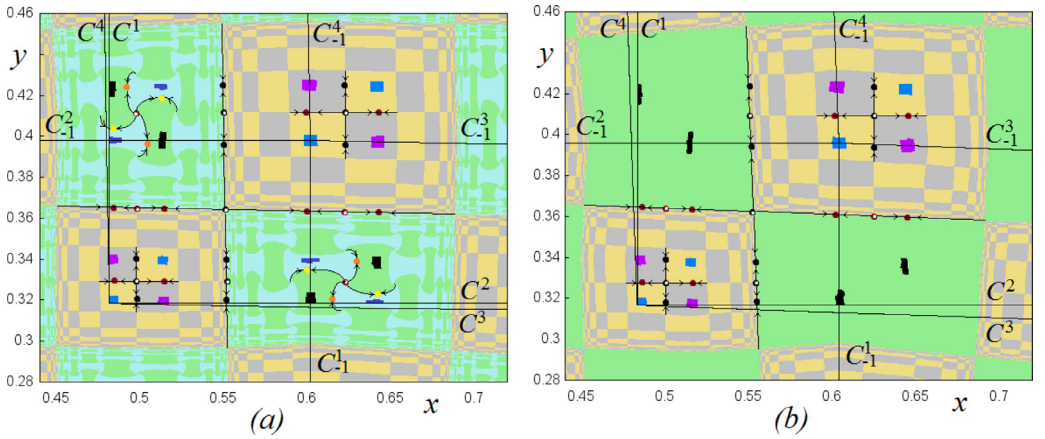

Fig. 11. (a) Four and (b) three coexisting 4-cyclic chaotic attractors of map F and their basins. Here $\theta = 2.7$, $\delta = 0.8$, $s_X = 0.6$, $s_Y = 0.4$ and (a) $\rho = 0.01$, (b) $\rho = 0.02$. (For interpretation of the references to color in the text, the reader is referred to the web version of this article.)

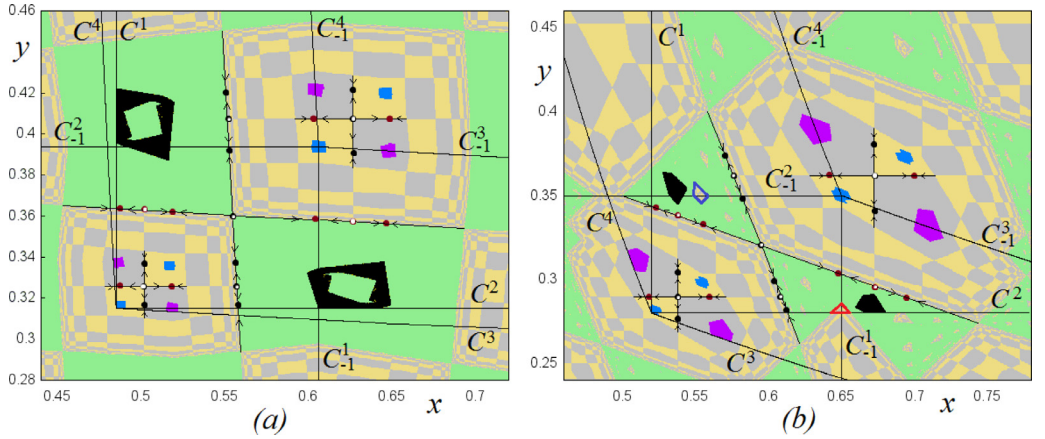

Fig. 12. Coexisting one 2-cyclic and two 4-cyclic chaotic attractors of map F and their basins for $\theta = 2.7$, $\delta = 0.8$, $s_X = 0.6$, $s_Y = 0.4$ and (a) $\rho = 0.03$, (b) $\rho = 0.2$. (For interpretation of the references to color in the text, the reader is referred to the web version of this article.)

4.2. Increasing ρ in the asymmetric case ($s_X \neq s_Y$)

Let the symmetry of map F be broken, that is, let $s_X \neq s_Y$, for example, $s_X = 0.6$, $s_Y = 0.4$. To describe some peculiarities of the bifurcation sequences observed in map F in the asymmetric case for ρ increasing in the range $0 < \rho < s_Y/s_X = 2/3$, we consider, as a starting point, four coexisting 4-cyclic chaotic attractors shown in Fig. 4a, where $\theta = 2.7$, $\delta = 0.8$, $\rho = 0$. Note that two of these attractors, namely, those shown in light blue and magenta, are synchronized (in the sense defined before), and two other attractors (shown in dark blue and black) are asynchronized.

At $\rho = 0.01$ map F still has four coexisting 4-cyclic chaotic attractors: we show them in Fig. 11a together with their basins whose boundaries are formed by the closure of the stable invariant sets of the related saddle 4-cycles. Increasing ρ further, one of the asynchronized 4-cyclic attractors (shown dark blue in Fig. 11a) has a contact with its immediate basin boundary and is transformed into a chaotic repellor, so that three coexisting 4-cyclic chaotic attractors are left (see Fig. 11b where $\rho = 0.02$). At $\rho \approx 0.024$ the asynchronized attractor shown in black in Fig. 11b also has a contact with its immediate basin boundary and undergoes an expansion bifurcation becoming a 2-cyclic annular chaotic attractor (see Fig. 12a where $\rho = 0.03$).

Fig. 12b presents the attractors of F for $\rho = 0.2$: the 2-cyclic asynchronized chaotic attractor, which has no longer an annular shape, is decreased in size while one of the 4-cyclic chaotic attractors (shown in magenta) is increased in size. Note that there are islands of the basins of the synchronized 4-cyclic chaotic attractors (shown in light blue and magenta) inside the basin of the asynchronized 2-cyclic chaotic attractor (shown in black). These islands are created due to the part of the basins (highlighted in red in Fig. 12b) of the 4-cyclic attractors, which 'entered' the region Z_4 after crossing the critical line C^2, leading to the appearance of new preimages of this part. In particular, one of these preimages (highlighted in blue) is intersected by C^2_{-1}.

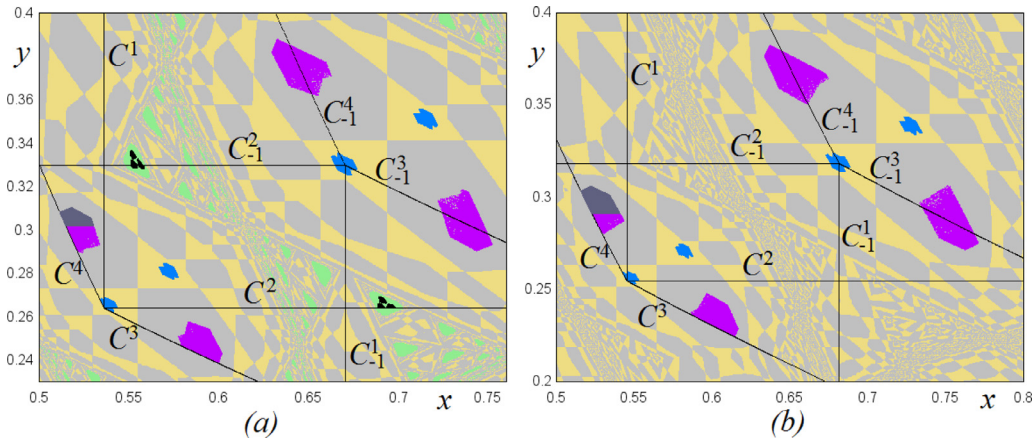

Fig. 13. (a) Two 4-cyclic chaotic attractors coexisting in with the asynchronized 6-cyclic chaotic attractor; (b) two 4-cyclic chaotic attractors. The 4-cyclic chaotic attractor shown in light blue is synchronized; the parts of the other 4-cyclic chaotic attractor, shown in magenta and dark gray are associated with the synchronized and asynchronized behavior, respectively. Here $\theta = 2.7$, $\delta = 0.8$, $s_X = 0.6$, $s_Y = 0.4$ and (a) $\rho = 0.26$, (b) $\rho = 0.29$. (For interpretation of the references to color in this figure legend, the reader is referred to the web version of this article.)

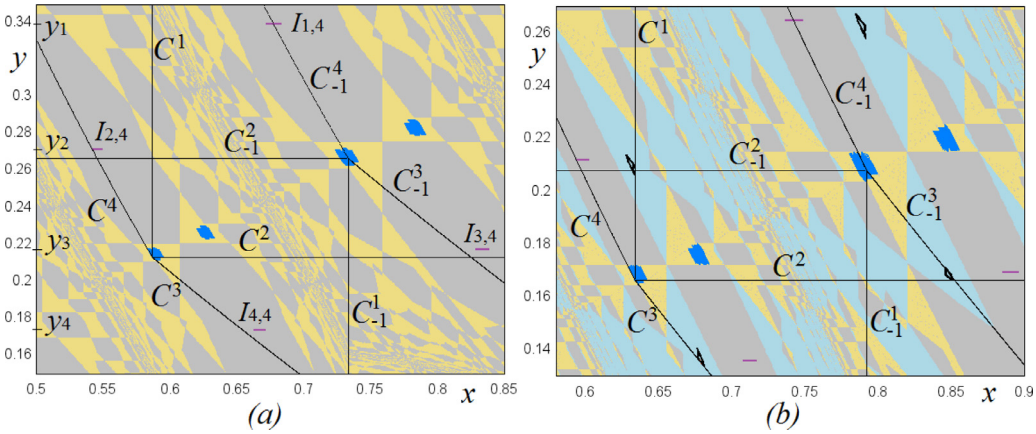

Fig. 14. (a) Coexisting synchronised 4-cyclic chaotic attractor and 4-cyclic chaotic intervals $I_4 = \{I_{i,4}\}_{i=1}^4$ and their basins; (b) additionally, map F has a 4-cyclic annular chaotic attractor. Here $\theta = 2.7$, $\delta = 0.8$, $s_X = 0.6$,$s_Y = 0.4$ and (a) $\rho = 0.4$, (b) $\rho = 0.49$. (For interpretation of the references to color in the text, the reader is referred to the web version of this article.)

Increasing ρ, the asynchronized 2-cyclic chaotic attractor decreases in size and is transformed via a reverse expansion bifurcation into a 6 -cyclic chaotic attractor (see Fig. 13a where $\rho = 0.26$). Then this 6-cyclic attractor is transformed (via an expansion bifurcation) back to a 2-cyclic attractor which continues to decrease in size and then disappears due to a BCB, so that at $\rho = 0.29$ map F has only two 4-cyclic chaotic attractors (see Fig. 13b).

Increasing ρ further the 4-cyclic chaotic attractor shown magenta in Fig. 13 decreases in size and at $\rho \approx 0.375$ it is transformed into 4-cyclic chaotic intervals $I_4 = \{I_{i,4}\}_{i=1}^4$ (see an example in Fig. 14a where $\rho = 0.4$). To explain a mechanism of such a transformation note that interval $I_{1,4}$ intersects the switching manifold C_{-1}^4, so, it has parts in both regions D_{HH} and D_{LH}; interval $I_{2,4} = F(I_{1,4})$ is folded along C^4 and $I_{2,4} \subset D_{LH}$; $I_{3,4} = F(I_{2,4}) \subset D_{HH}$ and $I_{4,4} = F(I_{3,4}) \subset D_{LL}$. Thus, map $G = F^4$ associated with attractor I_4 is a composition of the maps F_{LL}, F_{HH} and F_{LH} only, for which the dynamics of the variable y is independent on x, being defined by the functions $g_{LL}(y) = \delta(\theta s_Y(\rho) + (1-\theta)y)$ and $g_H(y) = \delta y$. Thus we can define map G as follows:

$$G : \begin{pmatrix} x \\ y \end{pmatrix} \to \begin{pmatrix} f(x,y) \\ g(y) \end{pmatrix},$$

which is a *triangular map*. Recall that $g(y)$ and $f(x, y)$ are called driving and driven maps, respectively.

Let us show that in the considered case the driving map g has an attracting fixed point. Consider an initial point $(x_1, y_1) \in D_{HH} \cup D_{LH}$. Then for the y-coordinates of its images the following holds: $y_2 = \delta y_1$; if $(x_2, y_2) \in D_{LH}$ then $y_3 = \delta^2 y_1$; if $(x_3, y_3) \in D_{HH}$ then $y_4 = \delta^3 y_1$; if $(x_4, y_4) \in D_{LL}$ then $y_5 = \delta(\theta s_Y(\rho) + (1-\theta)\delta^3 y_1)$, and if $(x_5, y_5) \in D_{HH} \cup D_{LH}$, that is, if the trajectory is back to the starting region (all the conditions listed above are satisfied for $(x_1, y_1) \in I_{1,4}$), one can consider the

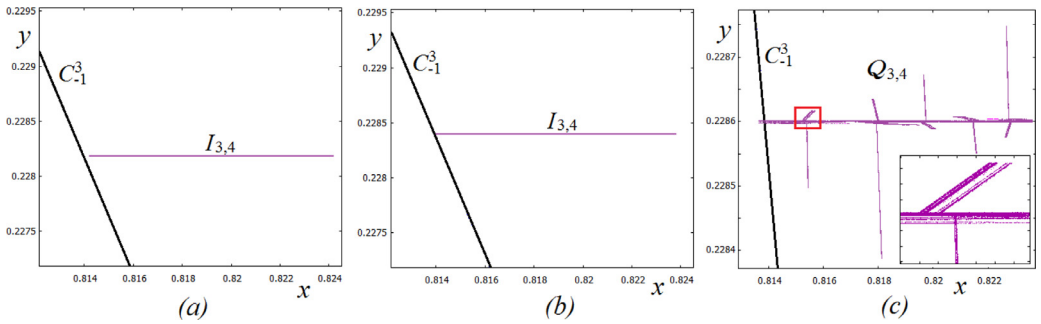

Fig. 15. One of the pieces of the 4-cyclic chaotic attractor of F undergoing a collision with the switching manifold C^3_{-1} and increasing its dimension. Here $\theta = 2.7$, $\delta = 0.8$, $s_X = 0.6$, $s_Y = 0.4$ and (a) $\rho = 0.375$, (b) $\rho = 0.3745$ and (c) $\rho = 0.374$. An inset in (c) shows the indicated rectangle enlarged.

map

$$g : y \mapsto g(y) = g_{LL} \circ g_H^3(y) = \delta\theta s_Y(\rho) + (1-\theta)\delta^4 y.$$

It has a fixed point $y^* = \delta\theta s_Y(\rho)/(1-(1-\theta)\delta^4)$ which is attracting for $\left|(1-\theta)\delta^4\right| < 1$, that is, for $0 < \theta < 1 + 1/\delta^4$. For the considered parameter values, that is, for $\theta = 2.7$, $\delta = 0.8$, $\rho = 0.4$ and $s_Y = 0.4$, it holds that the fixed point $y^* = y_1 \approx 0.3396$ is attracting. Thus, map G has a transversely attracting layer defined by $y = y_1$, the dynamics on which is governed by the driven map $f(x, y_1) =: f_1(x)$ which is the skew tent map defined as follows:

$$f_1 : x \mapsto \begin{cases} f_{1L}(x) = f_{LL} \circ f_H \circ f_{1LH} \circ f_H(x), & x \geq h_1(y_1), \\ f_{1H}(x) = f_{LL} \circ f_H \circ f_{1LH}^2(x), & x < h_1(y_1), \end{cases}$$

where $f_{LH}(x, y_1) =: f_{1LH}(x)$. The slopes of the linear branches of f_1 are $a_L = \delta^4(1-\theta)^2 > 0$ and $a_H = \delta^4(1-\theta)^3 < 0$. It is known that the skew tent map has a one-piece chaotic attractor (interval) if

$$a_L a_H + a_L - a_H > 0 \quad \text{and} \quad a_L a_H^2 + a_H - a_L > 0.$$

That is, for map f_1 it must hold that

$$\delta^8(1-\theta)^6 - \theta > 0 \quad \text{and} \quad \delta^4(1-\theta)^3 + \theta > 0.$$

It is easy to check that for the considered parameter values these inequalities are satisfied, thus, map f_1 has a one-piece chaotic attractor, which is the interval $I_{1,4}$. Coming back to the map F, it holds that it has 4-cyclic chaotic intervals $I_{i,4}$, $i = \overline{1,4}$, each of which is located on the related transversely attracting layer defined by $y = y_i$ (see Fig. 14a).

The mechanism of appearance of the 4-cyclic chaotic intervals I_4 can be commented for decreasing ρ: At $\rho = 0.375$ the interval $I_{3,4}$ is near to a contact with the switching manifold C^3_{-1} (see Fig. 15a), at $\rho \approx 0.3745$ this interval contacts C^3_{-1} (see Fig. 15b) and then the attractor intersects C^3_{-1} (see Fig. 15c where $\rho = 0.374$), that is, the 4-cyclic chaotic attractor has already a part belonging to D_{HL}, thus, map F_{HL} becomes also involved into the asymptotic dynamics associated with this attractor. The related map F^4 is no longer triangular, and the attractor increases its dimension having at first a Cantor like structure (as, e.g., in Fig. 15c), and then it becomes a full measure chaotic attractor (as, e.g., the one shown in magenta in Fig. 13).

In Fig. 14b ,where $\rho = 0.49$, we present the 4-cyclic chaotic intervals I_4 coexisting with the synchronized 4-cyclic chaotic attractor (shown in blue) which is near to its final bifurcation, and a 4-cyclic annular chaotic attractor (shown in black) born after a sequence of bifurcations initiated by a fold BCB. For increasing ρ first the attractor shown in blue and then the attractor shown in black are transformed into chaotic repellors due to a contact with their immediate basin boundaries, and the only attractor of map F, up to the limit value $\rho = 2/3$, is the 4-cyclic chaotic intervals I_4.

5. Conclusions

We considered a 2D continuous noninvertible piecewise smooth map, which characterizes the dynamics of innovation activities in the two-country model of trade and product innovation proposed by Matsuyama et al. [7], in which this map was derived from the underlying economic model, but also the case of two coexisting attracting 2-cycles was considered in detail, and it was shown that a gradual reduction in the trade cost, or globalization, causes a synchronization of endogenous innovation cycles across the two countries, in the sense that the basin of attraction of the synchronized 2-cycle expands and the basic of attraction of the asynchronized 2-cycle shrinks and eventually disappears. In the present paper we discussed a few bifurcation scenarios associated with chaotic attractors, which are interesting from the point of view of nonlinear dynamics theory. These scenarios involve border collision, merging, expansion and final bifurcations of various coexisting chaotic attractors, accompanied by transformations of their basins of attraction. We have seen that such peculiarities of map F as its nonsmoothness and noninvertibility essentially enrich the dynamics of the map. We have recalled the concept of

critical lines which are helpful in determining the boundaries of chaotic attractors, as well as in explaining some transformations in the structure of the basins. We have also unfolded a mechanism of peculiar border collision bifurcation of a chaotic attractor leading to an increase of its dimension.

Needless to say, this paper is just a first step towards a full characterization of the map developed in [7] and many important problems still remain to be addressed. Our analysis here already revealed that the map has a richer set of bifurcation scenarios than our earlier analysis of the 2-cycle case had identified. But, what has been reported in this paper is merely tips of the iceberg. There might still be many alternative "routes to synchronization" that we have not discovered. To be able to address this issue in a fully satisfactory manner, it is necessary to understand the properties of this map for the full set of the parameter space. We hope to address this and other remaining issues related to this map in our future work.

Acknowledgments

The work of L. Gardini and I. Sushko has been performed under the auspices of the COST Action IS1104 "The EU in the new complex geography of economic systems: models, tools and policy evaluation", and in the framework of the research project on "Dynamic Models for behavioral economics" financed by DESP, University of Urbino. I. Sushko thanks also University of Urbino for the hospitality during her stay there as a Visiting Professor.

References

[1] Avrutin V, Gardini L, Schanz M, Sushko I. Bifurcations of chaotic attractors in one-dimensional maps. Int J Bifurc Chaos 2014;24:1440012. (10 pages).
[2] Gardini L. Homoclinic bifurcations in n-dimensional endomorphisms, due to expanding periodic points. Nonlinear Anal Theory Methods Appl 1994;23(8):1039–89.
[3] Deneckere R, Judd K. Cyclical and chaotic behavior in a dynamic equilibrium model, chapter 14. Cycles and chaos in economic equilibrium. Benhabib Jess, editor. Princeton: Princeton University Press; 1992.
[4] Helpman E, Krugman P. Market structure and international trade. MIT Press, Cambridge; 1985.
[5] Ito S, Tanaka S, Nakada H. On unimodal transformations and chaos II. Tokyo J Math 1979;2:241–59.
[6] Maistrenko YL, Maistrenko VL, Chua LO. Cycles of chaotic intervals in a time-delayed Chua's circuit. Int J Bifurc Chaos 1993;3. 1557–72.
[7] Matsuyama K, Sushko I, Gardini L. Globalization and synchronization of innovation cycles. Geocomplexity: discussion papers series; 2015. No. 9/2015.
[8] Mira C, Gardini L, Barugola A, Cathala JC. Chaotic dynamics in two- dimensional nonivertible maps. World Scientific; 1996.
[9] Mira C, Fournier-Prunaret D, Gardini L, Kawakami H, Cathala JC. Basin bifurcations of two-dimensional noninvertible maps. Fractalization Basins Int J Bifurc Chaos 1994;4(2):343–81.
[10] Mira C, Carcasses JP, Gilles M, Gardini L. Plane foliation of two-dimensional noninvertible maps. Int J Bifurc Chaos 1996;6(8):1439–62.
[11] Nusse HE, Yorke JA. Border-collision bifurcations including period two to period three for piecewise smooth systems. Physica D 1992;57:39–57.
[12] Sushko I, Gardini L. Degenerate bifurcations and border collisions in piecewise smooth 1D and 2D maps. Int J Bifurc Chaos 2010;20:2046–70.
[13] Sushko I, Avrutin V, Gardini L. Bifurcation structure in the skew tent map and its application as a border collision normal form. J Differ Equ Appl 2015. doi:10.1080/10236198.2015.1113273.